Bull Volcanol (1999) 61:32–39

ORIGINAL PAPER

M. S. Ramsey · J. H. Fink

Estimating silicic lava vesicularity with thermal remote sensing: a new technique for volcanic mapping and monitoring

Received: 25 June 1998 / Accepted: 14 December 1998

Abstract Remote monitoring of active lava domes provides insights into the duration of continued lava extrusion and detection of potentially associated explosive activity. On inactive flows, variations in surface texture ranging from dense glass to highly vesicular pumice can be related to emplacement time, volatile content, and internal structure. Pumiceous surface textures also produce changes in thermal emission spectra that are clearly distinguishable using remote sensing. Spectrally, the textures describe a continuum consisting of two pure end members, obsidian and vesicles. The distinct spectral features of obsidian are commonly muted in pumice due to overprinting by the vesicles, which mimic spectrally neutral blackbody emitters. Assuming that this energy combines linearly in direct proportion to the percentage of vesicles, the surface vesicularity can be estimated by modeling the pumice spectrum as a linear combination of the glass and blackbody spectra. Based on this discovery, a linear retrieval model using a least-squares fitting approach was applied to airborne thermal infrared data of the Little Glass Mountain and Crater Glass rhyolite flows at Medicine Lake Volcano (California) as a case study. The model produced a vesicularity image of the flow with values from 0 to ~70%, which can be grouped into three broad textural classes: dense obsidian, finely vesicular pumice, and coarsely vesicular pumice. Values extracted from the image compare well with those derived from SEM analysis of collected samples as well as with previously reported results. This technique provides the means to accurately map the areal distributions of these textures, resulting in significantly different values from those derived using aerial photographs. If applied to actively deforming domes, this technique will provide volcanologists with an opportunity to monitor dome-wide degassing and eruptive potential in near-real-time. In July 1999 such an effort will be possible for the first time when repetitive, global, multispectral thermal infrared data become available with the launch of the Advanced Spaceborne Thermal Emission and Reflectance Radiometer (ASTER) instrument aboard the Earth Observing System satellite.

Key words Remote sensing · Vesicularity · Explosive eruptions · Monitoring · Hazards

Editorial responsibility: S. Carey

Michael S. Ramsey (✉) · Jonathan H. Fink
Department of Geology, Arizona State University, Box 871404, Tempe, Arizona 85287–1404, USA
Fax: +602 965 1787
e-mail: ramsey@elwood.la.asu.edu

Introduction

Remote sensing provides spectral, spatial, and temporal coverage for both geologic mapping and monitoring at numerous volcanoes throughout the world. The use of satellites and aircraft to monitor active volcanic sites and map the products of eruptions has been ongoing for decades. Progressively more complex image processing techniques have been applied to an increasing number of data sets to derive such characteristics as the amount of magmatic inflation of a region using interferometric radar (Rosen et al. 1996), the presence of hot spots with short-wave infrared (Abrams et al. 1991), and the volume of sulfur dioxide in plumes using thermal infrared (TIR; Realmuto et al. 1994). Such monitoring programs, designed to mitigate volcanic hazards, will need to be expanded in the future as population centers continue to encroach upon dangerous volcanoes.

If one were to select volcanologic remote sensing targets of potential hazards on the basis of where the largest numbers of people have recently been killed or are currently threatened, frequently observed basaltic shield volcanoes such as Kilauea (Hawai‘i) would be replaced by more silicic volcanoes such as Merapi (Indonesia), Santa Maria (Guatemala), Unzen (Japan), Mount St. Helens and Augustine (United States), Galeras (Colombia), and Soufriere Hills (Montserrat). Recent activity at these seven volcanoes has been characterized by the emplacement of andesite or dacite lava domes whose growth and collapse have killed thousands of people this century (Rothery 1989). Over a longer time span, volcanoes such as these also have the potential to undergo large-scale sector collapse or caldera formation, which could lead to tens of thousands of fatalities.

Current remote sensing platforms are limited in many ways for systematic volcano monitoring. Spaceborne instruments provide data from remote regions but with poor spectral or spatial resolution. Airborne instruments, on the other hand, have the advantage of higher resolutions but lack the ability to engage in long-term observations, especially in remote regions. The ASTER instrument scheduled for launch in July 1999 will provide continuous global observations spanning three wavelength regions from the visible to the thermal infrared (Kahle et al. 1991). High spatial and moderate spectral resolution data will allow monitoring of changes in dome morphology, composition, and temperature. For over-steepened domes, these changes may signal flow-front collapse that can generate pyroclastic flows and debris avalanches (Fink and Kieffer 1993).

Past remote sensing studies of volcanic products have measured parameters such as the aspect ratio, length, and roughness (Campbell and Garvin 1993; Rowland et al. 1994; Plaut et al. 1995). An important lava property previously neglected is surface vesicularity. Vesicularity can be used to infer pre-eruptive conditions affected by the volatile content, emplacement time, and internal structure of the flow. Although factors such as vesicle size and the scattering physics of reflected solar energy may complicate remote sensing analyses, pumiceous textures produce significant variations in thermal emission spectra that are clearly distinguishable (Fig. 1).

The effect of silicic pumice textures on emitted energy has been explored by Ondrusek et al. (1993). Using both high-resolution laboratory emission spectroscopy and airborne TIR data of Little Glass Mountain, they first showed that both coarsely vesicular pumice (CVP) and finely vesicular pumice (FVP) have shallower spectral features than does dense obsidian (OBS). This reduction in spectral contrast was attributed to progressively more contamination by blackbody (absorption-free) energy with increasing vesicularity. Using a simple band ratio technique, they were able to distinguish FVP from CVP. However, due to the low spatial resolution of the data and the simplicity of the technique, no identification of OBS or quantitative estimation of vesicle percentage was possible.

This paper describes our use of TIR remote sensing and a recently developed analytical model (Ramsey and Christensen 1998) to estimate the surface vesicularity of the Little Glass Mountain rhyolite flow in northern California. This approach lays the groundwork for future real-time monitoring of active summit domes and flows, which commonly appear as passive precursors or postscripts to large explosive eruptions.

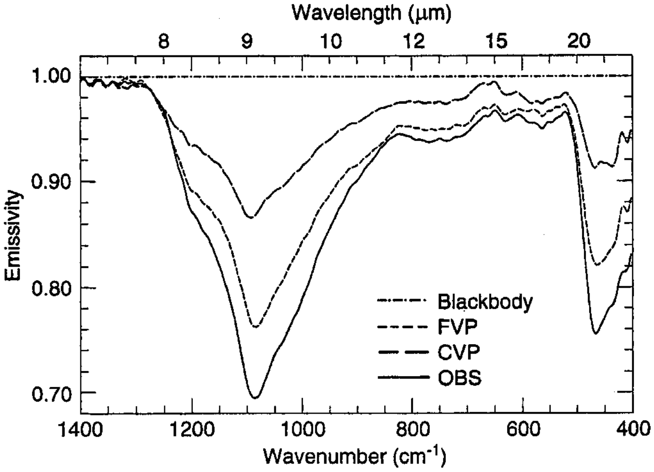

Fig. 1 Emission spectra of the units shown in Figs. 3–4 together with an emissivity equal to one representing an ideal blackbody. Spectra shown are averages of at least ten samples to account for orientation and weathered surface effects. The large absorption band at 9.25 μm is diagnostic of glass and is caused by the stretching vibrations of silica tetrahedra. The blackbody and obsidian (*OBS*) served as end members for the deconvolution model, which estimated the percentage of vesicles in the pumice based on the fit of the end-member spectra. *CVP* coarsely vesicular pumice; *FVP* finely vesicular pumice

Geologic setting

Medicine Lake is a large Quaternary shield volcano 55 km east–northeast of Mount Shasta in northern California (Fig. 2). It is located behind the main axis of Cascade stratovolcanoes in an extensional tectonic setting. The overall morphology of the volcano is controlled by voluminous older tholeiitic basalt flows erupted around the flanks of the volcano as recently as 1.1 ka (Donnelly-Nolan 1988). More silicic calc-alkaline lava flows began to appear in the past 4.3 ka and are found mainly within or immediately surrounding the summit caldera (Donnelly-Nolan et al. 1990). One of the largest of these is the Little Glass Mountain (LGM) flow, a 3.7 km^3 chemically homogeneous rhyolite ($\sim$74 wt.% SiO_2) that formed approximately 1.1 ka (Heiken 1978; Donnelly-Nolan et al. 1990). The LGM flow is formed by two coalescing domes that have vent orientations in line with a northeast-trending zone of ground cracks and the Crater Glass (CG) flow vents (Fink and Manley 1987; Donnelly-Nolan et al. 1990). The CG flows consist of a series of six smaller domes with a total volume of just over 1 km^3. The composition and age of the CG domes are indistinguishable from LGM, and both eruptions are considered contemporaneous (Heiken 1978).

The surfaces of these flows exhibit the three pumiceous textures commonly observed on silicic flows in

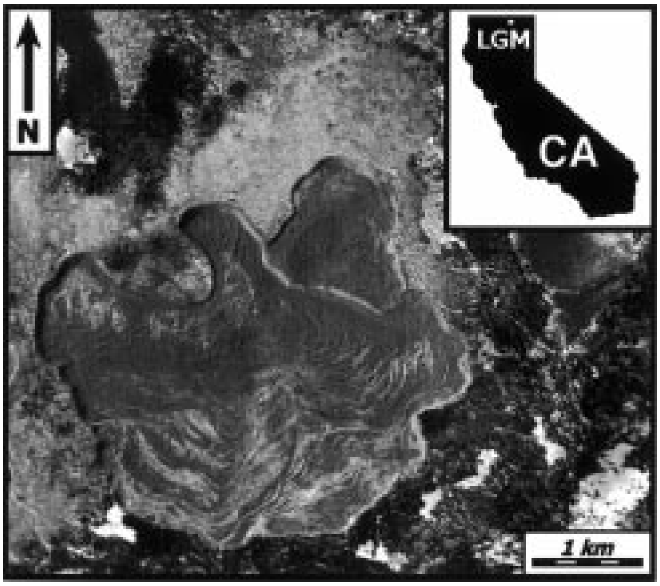

Fig. 2 TIMS-derived brightness temperature image of the Little Glass Mountain (*LGM*) rhyolite flow and surrounding area, with *inset* showing the flow's location. *Brighter regions* (warmer temperatures) in the image correlate to deformed CVP diapirs on the flow and to the surrounding pumice plain. *Darker areas* are cooler and correspond to surrounding vegetation, less vesicular FVP, and dense microcrystalline lava on the flow

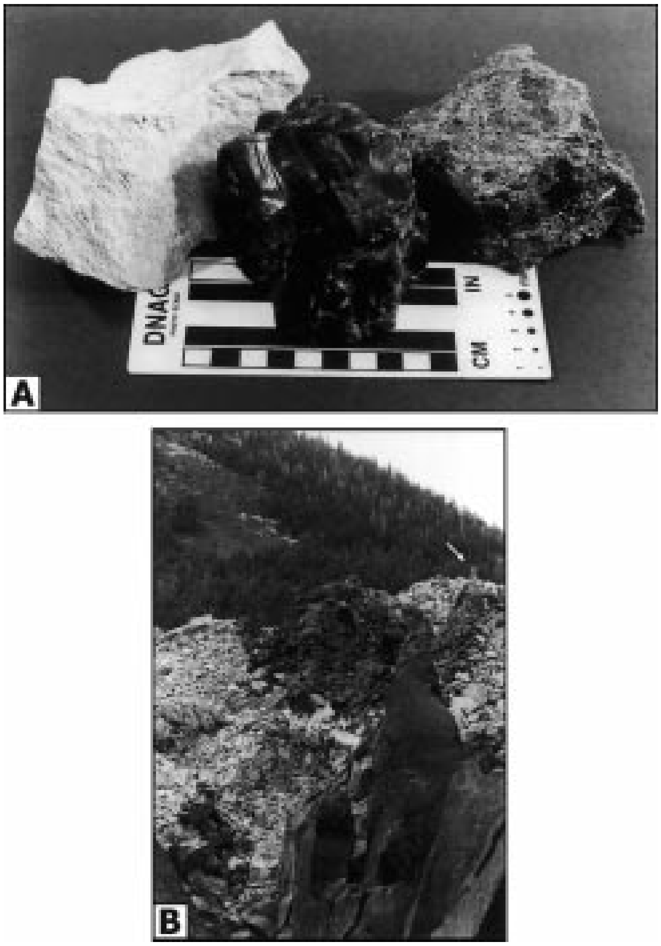

Fig. 3A, B Textural units described in text. **A** Hand samples of FVP (*left*), OBS (*middle*), and CVP (*right*) collected from LGM. **B** Typical exposures of two dark-colored CVP diapirs surrounded by thin zones of OBS and large areas of light-colored FVP. Photograph taken at LGM flow with *arrow* denoting person for scale

addition to a late-stage, dense (~10% vesicularity) microcrystalline lava that was emplaced over the vent locations (Fig. 3). Variations in vesicularity on silicic flows are caused in part by volatile distribution as well as lava emplacement and cooling. Fink and Manley (1987) examined drill cores through a young rhyolite flow to delineate three primary vesicular textures based on color and vesicle concentration: black obsidian (OBS; 0–10 vol %), light-colored finely vesicular pumice (FVP; 10–30 vol.%), and dark-gray coarsely vesicular pumice (CVP; 40–70 vol.%). The upper surfaces of rhyolite flows are commonly comprised of several meters of FVP, which consists of small (<0.5 mm), non-connected, jagged vesicles (Fig. 4; Fink 1983; Sampson 1987). Below the FVP is a zone of non-vesicular OBS, which is also exposed in distinct layers along the flow margins and adjacent to outcrops of CVP. The CVP forms in response to volatile migration and bubble coalescence due to shear during flow (Fink and Manley 1987). As a result, the vesicles are smooth-walled, dis-

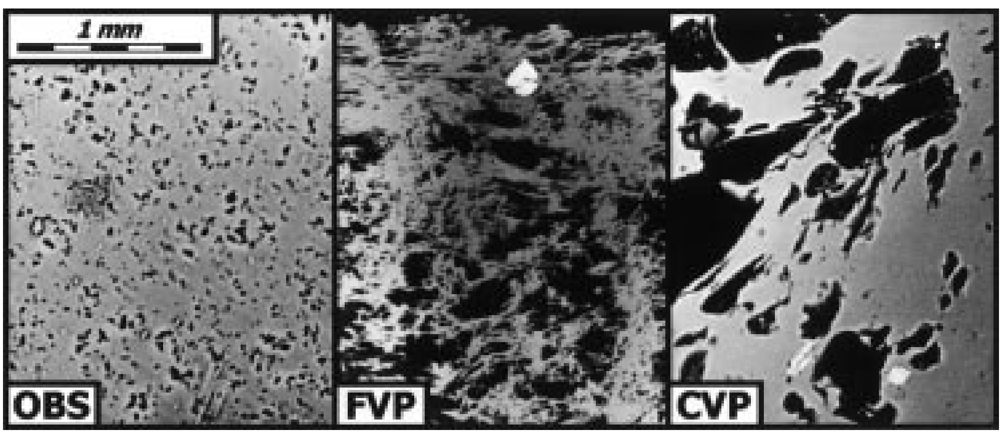

Fig. 4 SEM photomicrographs of the primary pumice textures exposed on rhyolite flow surfaces (*OBS, FVP, CVP*). Note the different size, shape, and connectedness of the vesicles in FVP and CVP. These factors influence the spectral contrast of the thermal infrared absorption bands

torted, and much larger (1–10 mm) than those in FVP (Fig. 4). Bubbles commonly form more than 50% of the volume of CVP, leading to a density contrast with the overlying OBS. This allows the CVP to rise buoyantly, producing distinctive diapiric outcrops on the surface surrounded by the pierced OBS layer (Fink 1983). The diapirs range in size from $\sim$5 m to >1 km and are commonly deformed during the advance of the flow. Where volatile migration and bubble formation occur rapidly, diapiric rise gives way to rapid decompression and the formation of explosion pits.

Recently active dacite and andesite domes also display variations in surface vesicularity, though not to the extent of rhyolite (Fig. 5). For example, Anderson and Fink (1990) mapped two distinct lava textures on the Mount St. Helens' dome following the 1980 eruption: smooth (<15 vol.%) and scoriaceous (>50 vol.%). Similar textures were documented at Unzen volcano during the dome growth phase (Nakata et al. 1995). As in the case of Unzen, endogenous growth of lava domes on steep slopes or with volatile-enriched interiors have the increased potential of explosive collapse that might initiate pyroclastic activity (Fink and Kieffer 1993). Because vesicularity can be used to infer variations in volatile content on silicic flows, monitoring vesicularity changes using remote sensing can provide the ability to forecast the effects of renewed explosivity.

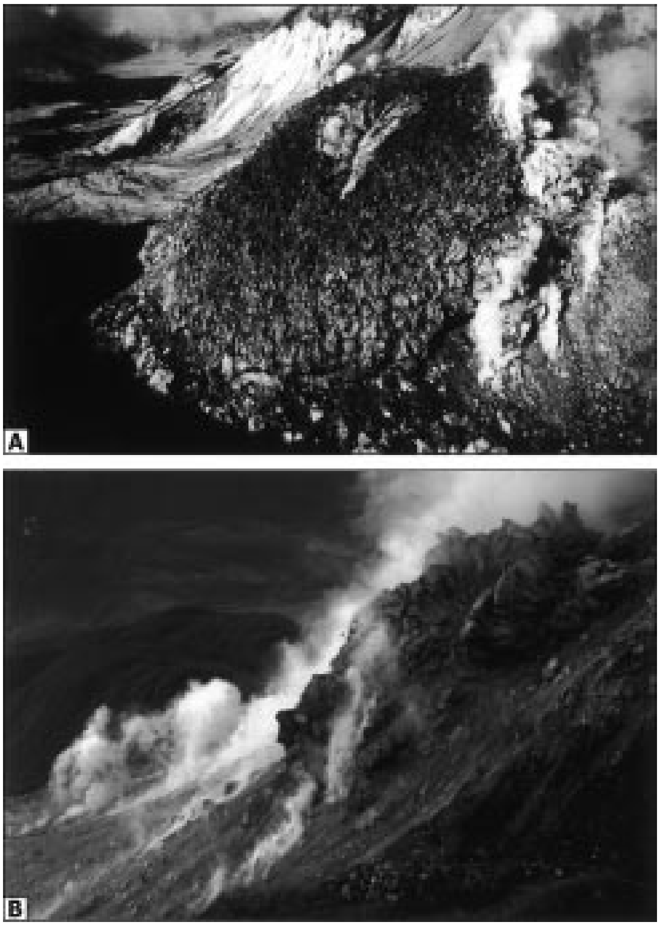

Fig. 5 **A** June 1981 Mount St. Helens lava dome (photo courtesy of the USGS). Two different textures are evident on the active lobe: a highly vesicular "scoriaceous" lava containing $\sim$50% vesicles, and a relatively non-vesicular "smooth" lava containing <15% vesicles (Anderson and Fink 1990). **B** March 1992 Unzen lava dome being emplaced at a steep angle. Numerous collapse events of the dome were responsible for deadly pyroclastic flows

Spectral analysis and model

The prominent absorption bands (emissivity lows) in thermal emission spectra of crystalline silicate minerals occur between 7 and 11 μm and are caused by the vibrational harmonics of the Si–O bonds (Salisbury 1993). In general, the feature width is inversely proportional to the degree of uniformity of the bond strengths (Simon and McMahon 1953). These features are evident in the emission spectra of silicate glasses as well. However, the rapid quenching of the melt results in a lack of long-range structural order and randomness of the silica tetrahedra. This alteration of the fundamental structural makeup of a mineral due to vitrification causes a broadening and widening of the absorption bands together with the loss of most small-scale features (Nash and Salisbury 1991; Ramsey et al. 1993). Typically, glassy lavas will contain only two prominent features in the 7- to 25-μm wavelength region (Fig. 1). The first, a broad V-shaped absorption band spanning 8–12 μm, is attributed to the stretching vibrations of silica tetrahedra and is detectable within the Earth's atmospheric window (8–13 μm). The second dominant absorption band occurs from 20–25 μm, well outside that window, and is therefore unavailable for remote sensing purposes.

Although the reduction in contrast in pumice spectra mimics the effects of simple addition of a blackbody radiator, the behavior is more complex. Vesicles exposed at the surface create cavities that are generally many times the size of the emitted energy's wavelength. Therefore, photons are free to interact with one or more cavity surfaces, undergoing multiple reflections before being absorbed. Because the reflected energy (R) is related to the emitted energy ( ) such that R = 1- , any amount of added reflected energy will increase the emissivity at the absorption bands (Fig. 1) and thus approximate an ideal (blackbody) radiator. A similar phenomenon is observed in emission studies of fine particle sizes, where emitted photons are able to interact with progressively more reflecting surfaces (Ramsey and Christensen 1998; Mustard and Hays 1997). If the photon path is convoluted and the number of reflections high (as for pumice vesicles), the emitted energy will contain very shallow absorption bands and can therefore be approximated as the spectra of non-vesicular glass plus blackbody.

On pumiceous surfaces, the intimate mixing of emitted energy from glass and vesicles requires a quantitative technique more sophisticated than a band ratio in order to separate the contribution of each. Assuming the emitted energy from the glass and vesicles combines linearly, then a least-squares (deconvolution) model can be used to map the surface distribution and percentage of vesicles for each textural unit. The premise that emitted thermal energy from multiple components on a surface mixes linearly with respect to their areal abundance has been validated by several authors (Thomson and Salisbury 1993; Ramsey and Christensen 1998). This fundamental property of infrared spectroscopy provides the means to identify the type and percentage of end members below the resolution of the TIR instrument, assuming the spectra of those end members are known (i.e., a spectral library). In this case, vesicularity rather than mineralogy is being derived by way of the blackbody end member. Spectra of glassy flows throughout the western United States, Hawai'i, and Central America have been examined over the course of this investigation. The data set is remarkably uniform, with variations in emission feature morphology of less than ~5%. This justifies the use of the end-member spectra (Fig. 1) chosen for this study and should allow a common glass end member to be used for data of remote flows using ASTER.

The deconvolution algorithm linearly fits the end-member spectra to the unknown pumice spectrum in each pixel of the image to produce an end-member abundance map, as well as a root-mean-squared (RMS) error image. The RMS image is a measure of the misfit of the model summed over the entire wavelength region and indicates areas of poor model fit. These are regions not fit by the chosen end members and therefore investigated further or ignored if not of direct interest.

Methodology

Samples from the LGM flow were collected during the summers of 1993–1995. High-resolution laboratory spectra of each were acquired at the Arizona State University Thermal Emission Spectrometer Laboratory (Ruff et al. 1997). Data were taken from fresh and weathered surfaces as well as at several different sample orientations in order to quantify the magnitude of these effects. The spectra shown in Fig. 1 were derived from the 2-cm spot size of the spectrometer and were averaged to represent the many different vesicle orientations present on the surface of the flow. The linear deconvolution model, originally developed to detect mineralogic variations (Ramsey and Fink 1994; Ramsey and Christensen 1998), was adapted for use as a textural detection algorithm. Prior to image analysis, the model was applied to the laboratory data and the resulting vesicularity estimate, model fit, and error were used to determine the accuracy and obtain a point of comparison for the image results. The model-derived vesicularity for the laboratory and TIR imagery was also compared with previously published values and SEM-derived averages (Table 1). The SEM photomicrographs shown in Fig. 4 were taken from samples collected at Obsidian Dome, Long Valley Caldera, California, from the same textural units as those at LGM. Vesicularity values were estimated based on the percentage of void spaces in the upper 1 mm of each photomicrograph.

The remote sensing portion of this study used airborne data from the NASA Thermal Infrared Multispectral Scanner (TIMS). The TIMS instrument is designed to operate within the TIR atmospheric window, collecting six spectral channels of emitted thermal radiance from the ground surface and intervening atmospheric column (Kahle and Goetz 1983). The resolution of each image pixel depends on the aircraft altitude and instrument field of view. The data presented here, with a resolution of 10.4 m/pixel, were acquired in July 1989 from the same flight line used by Ondrusek et al. (1993). Surface units, having different compositions or textures and an areal extent smaller than the image resolution, are detected as one composite spectrum per pixel. This spectrum also contains information on the ground temperature and intervening atmosphere between the surface and sensor.

Several processing and calibration steps were performed to reduce the data to the wavelength-dependent surface emissivity. Atmospheric absorption was removed using the MODTRAN radiative transfer model with a standard mid-latitude summer profile (Berke et al. 1989). Upon atmospheric correction, the calibrated surface radiance is reduced to a combination of the brightness temperature and emissivity. Using the emissivity-temperature separation technique described by Realmuto (1990), the data were divided into one brightness temperature (Fig. 2) and six emissivity images. As for the laboratory data, the emissivity derived from the TIMS relates directly to surface proper-

Table 1 Vesicularity values of silicic pumice textures. *OBS* obsidian; *FVP* finely vesicular pumice; *CVP* coarsely vesicular pumice; *n.d.* not determined

	OBS (%)	FVP (%)	CVP (%)
Previous work			
Fink (1983)[a]	n.d.	≈30	≈50
Fink et al. (1992)[b]	0	30	20
Sampson (1987)[c]	0	≈30	≥50
This work			
SEM analysis	0–5	25–42	37–54
Laboratory resolution	0	25–33	43–65
TIMS resolution[d]	0	28–39	46–70

[a] Estimated values based on SEM photomicrographs
[b] Determined from SEM images of drill core samples of Obsidian Dome, Long Valley, California. Low CVP value is the result of bubble compression at the sample depth of approximately 18 m
[c] Average values from the Inyo Domes, Long Valley Caldera, California
[d] Values determined from a nine-pixel average

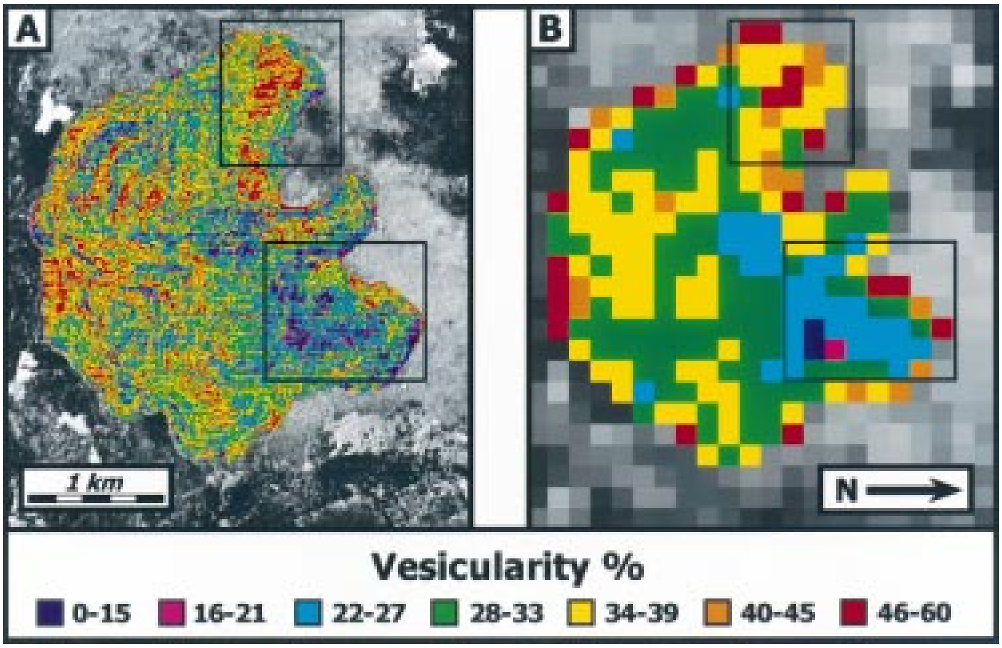

Fig. 6 Vesicularity maps of LGM at **A** 10.4 m/pixel resolution (TIMS) and **B** 90 m/pixel resolution (simulated ASTER) derived from the linear deconvolution of the emissivity images. The areal percentage of vesicles have been grouped into color-coded ranges for ease of viewing. Areas of *red* and *orange* denote outcrops of CVP, *green* and *yellow* correspond to the more abundant FVP, and *blue* and *magenta* indicate OBS and dense microcrystalline lava. *Boxed regions* show areas of high and low vesicularity and are visible in both data sets. On active domes, regions of high vesicularity have the increased potential of subsequent explosive eruptions and should be targeted for intense monitoring using ASTER

ties and serves as an input into the deconvolution model.

The laboratory-derived spectra (Fig. 1) were reduced to the six-point TIMS spectral resolution. With the OBS and a blackbody serving as spectral end members, the model was utilized to produce a vesicle-percentage image for the dome (Fig. 6). Average values from areas of known surface texture were extracted from this image and compared with the laboratory results and previously reported values. Finally, the image was color coded based on narrow vesicularity increments and also degraded from 10.4 to the 90-m resolution of the TIR portion of ASTER. This allowed for an estimate of the model's suitability for future spaceborne monitoring.

Results

Using the OBS and blackbody spectra as end members, the CVP and FVP laboratory spectra for all the samples were deconvolved (Table 1). Values for the FVP range from 25 to 33% with an average of 29%. These compare well with previous estimates based on petrography and also fall within the range calculated from the SEM analysis. Model-predicted vesicularity values for the CVP samples are 43 to 70% with an average of 59%. Upon visual inspection, the overall fit of the model-derived spectrum is excellent for all samples. This is confirmed by examining the model error, which shows very little wavelength-dependant deviation and an average RMS value of 0.51% emissivity. This is the same order of magnitude as errors from mineral mixtures taken under ideal conditions (Ramsey and Christensen 1998).

Depending on viewing geometry of a sample with respect to the spectrometer, spectral features vary to a small degree (<10%). This variation in the depth of the features is due to a change in the ratio of vesicles to glass detected by the spectrometer. The effect is most prominent in samples with deformed and elongated vesicles that present one surface of nearly pure glass and another of mainly vesicles. For spectra of these samples, lower model values (vesicularity underestimates) were derived, because fewer vesicles and more glass were observed. Because pure blackbody emission is defined as Lambertian (radiation emitted equally in all directions), the observed spectral change in these samples indicates that the vesicles are not ideal blackbody emitters as postulated by Ondrusek et al. (1993). The energy clearly has a preferred angle of emission due to the reflected component within the vesicles. However, because of the random orientation of vesicles and blocks on the surface of a dome, this orientation effect is minimized and not a significant factor in remote sensing situations.

The same process translated to the TIMS data produced a vesicularity image map (Fig. 6). Shown in red, the CVP distribution is clearly visible as elongate bands on the southern and northwestern lobes. Along with the interspersed FVP zones, these correspond well with the maps of LGM presented in Fink and Manley (1987) but show far greater detail. For example, mapping the CVP distribution on a dome using only aerial photographs can be misleading, as both CVP and OBS are dark in color and the gradational transitions between CVP and FVP can be easily missed. This error is evident by comparing the amount of CVP (here defined as pumice >46% vesicularity) determined by this method with the values reported by Fink and Manly (1987). They estimate CVP covering ~31% of the surface of

LGM and ~20% of the Crater Glass domes to the north, whereas this technique results in 19.4 and 38.6%, respectively. Fink and Manley (1987) postulated that the amount of CVP exposed on the surface correlates with the overall size of the flow. However, based on the results presented here, size clearly is not the only controlling factor. The larger amount of CVP at the CG domes may have been due either to an increased volatile content or variations in the eruption rate or both.

The other primary surface textures are also detected on LGM. Sub-pixel exposures of OBS (<5% vesicularity) show up in the steep flow fronts and surrounding the larger CVP diapirs. Also shown in blue is the glassy dense microcrystalline lava (5–15% vesicularity) exposed over the vent regions. The errors associated with the model fit average less than 2% emissivity, indicating that the two textures were adequate to describe the spectral characteristics of the LGM flow surface. Nine-pixel averages were extracted from the image over different regions of the flow (Table 1). These values are slightly higher than those from the laboratory data and result from the degradation of the sharp spectral features at the lower TIMS resolution. Where degraded to the 90-m spatial resolution of the ASTER TIR spectrometer, the intricate detail of the flow's surface texture is no longer visible (Fig. 6b); however, many of the large-scale patterns are still evident. On active domes, regions of high vesicularity (such as the outlined northwest lobe) would clearly be detected and could be intensively monitored for potential explosive activity. The loss of detail can also be compensated to some degree by using the 15 m/pixel ASTER visible data. Overlaying the vesicularity maps onto the visible images and the ASTER-derived digital elevation model (DEM) product will serve to accurately locate sub-90 m textural changes (Ramsey et al. 1998).

Conclusion

The work presented here serves as a case study for the applicability of this technique to estimate the vesicularity of lava flow surfaces using thermal infrared remote sensing. Based on laboratory studies of high-resolution rhyolite pumice and glass spectra, the methodology was successfully translated to remote sensing data. Because of the volume of published information, the authors' experience, and the availability of TIMS data, Medicine Lake Volcano was chosen for this study. It also serves as a potential analog for active domes and flows without the complication of surface temperature anomalies and active degassing.

Textural variations on the surfaces of silicic domes and flows produce thermal infrared spectral differences that are interpretable as linear combinations of only two end members, glass and blackbody (Ramsey and Fink 1997). This recognition allows a deconvolution model to be applied in order to estimate surface vesicularity. The areal percentage of blackbody-like vesicles can be predicted, making the identification of textural units possible, which in turn can lead to a better understanding of the dome's emplacement and cooling. The sensitivity of the model also allows for slight variations in vesicle percentage within the same textural unit to be resolved, in effect producing a micro-scale surface roughness map. This approach appears to be valid for young glassy rhyolite flows, based on the small model errors and comparisons with other data sets.

This technique has the potential to be an extremely important tool for hazard assessment on active lava flows and can be used in conjunction with field work and laboratory analysis of samples for detailed studies of inactive flows. An understanding of the effects of different compositions on the model is important for other investigations. Therefore, expansion of this work is underway with image and field studies ongoing for the dacite lava domes at Medicine Lake and Mount St. Helens as well as for basaltic pahoehoe and a'a flows at Kilauea. For example, similar textural changes on the dome of Mount St. Helens from 1980–1986 (Fig. 5) and Unzen from 1993–1994 were used as indicators of eruption rate and endogenic growth (Anderson and Fink 1990; Nakada et al. 1995). In addition, changes in the vesiculation of pahoehoe flows have been used to estimate the inflation potential of recent basaltic lavas (Cashman and Kauahikaua 1997). Therefore, this technique could have far greater potential for use by investigators not directly involved with either remote sensing or silicic dome studies.

In situ measurements of active silicic domes are important, but they can be hindered by heat and gas emission and the threat of future explosive eruptions. The use of TIR remote sensing can help to mitigate these personal hazards and provides valuable information on changes in flow temperature and surface morphology. A rapid analysis technique, such as the one presented here, applied to future data from ASTER will aid in determining the potential of subsequent eruptive activity at active volcanoes.

Acknowledgements The authors thank J. Donnelly-Nolan, S. Anderson, R. Wessels, M. Poland, and S. Ruff for helpful discussions and/or field assistance, as well as the entire crew of the NASA C-130 aircraft program for their dedication in acquiring the TIMS data sets. This manuscript was improved through the helpful reviews of D. Crown, D. Swanson, and an anonymous reviewer. Research funding for this study was provided by NASA through the ASTER science project, the Solid Earth and Natural Hazards Research Program, and the Planetary Geology and Geophysics Program.

References

Abrams M, Glaze L, Sheridan M (1991) Monitoring Colima volcano, Mexico, using satellite data. Bull Volcanol 53:571–574

Anderson SW, Fink JH (1990) The development and distribution of lava textures at the Mount St. Helens dome. In: Fink JH (ed) Lava flows and domes: emplacement mechanisms and hazard implications. IAVCEI Proc Volcanol 2:25–46

Berke A, Bernstein LS, Robertson DC (1989) MODTRAN: a moderate-resolution for LOWTRAN 7. Air Force Sys Com Geophys Lab Rep GL-TR-89-0122, pp 1–137

Campbell BA, Garvin JB (1993) Lava flow topographic measurements for radar data interpretation. Geophys Res Lett 20:831–834

Cashman KV, Kauahikaua JP (1997) Reevaluation of vesicle distributions in basaltic lava flows. Geology 25:419–422

Donnelly-Nolan JM (1988) A magmatic model of Medicine Lake Volcano, California. J Geophys Res 93:4412–4420

Donnelly-Nolan JM, Champion DE, Miller CD, Grove TL, Trimble DA (1990) Post-11,000-year volcanism at Medicine Lake Volcano, Cascade Range, California. J Geophys Res 95:19693–19704

Fink JH (1983) Structure and emplacement of a rhyolitic obsidian flow: Little Glass Mountain, Medicine Lake Highland, California. Geol Soc Am Bull 94:362–380

Fink JH, Kieffer SW (1993) Explosive decompression of lava domes: estimates of pyroclastic flow velocities. Nature 363:612–615

Fink JH, Manley CR (1987) Origin of pumiceous and glassy textures in rhyolite flows and domes. In: Fink JH (ed) The emplacement of silicic domes and lava flows. Geol Soc Am Spec Pap 212:77–88

Heiken G (1978) Plinean-type eruption at the Medicine Lake Highland, California, and the nature of the underlying magma. J Volcanol Geotherm Res 4:375–402

Kahle AB, Goetz AFH (1983) Mineralogic information from a new airborne thermal infrared multispectral scanner. Science 222:24–27

Kahle AB, Palluconi FD, Hook SJ, Realmuto VJ, Bothwell G (1991) The advanced spaceborne thermal emission and reflectance radiometer (ASTER). Int J Imaging Syst Tech 3:144–156

Mustard JF, Hays JE (1997) Effects of hyperfine particles on reflectance spectra from 0.3 to 25 μm. Icarus 125:145–163

Nakada S, Miyake Y, Sato H, Oshima O, Fujinawa A (1995) Endogenous growth of dacite dome at Unzen volcano (Japan), 1993–1995. Geology 13:157–160

Nash DB, Salisbury JW (1991) Infrared reflectance spectra (2.2–15 μm) of plagioclase feldspars. Geophys Res Lett 18:1151–1154

Ondrusek J, Christensen PR, Fink JH (1993) Mapping the distribution of vesicular textures on silicic lavas using the Thermal Infrared Multispectral Scanner. J Geophys Res 98:15903–15908

Plaut JJ, Stofan ER, Anderson SW, Crown DA (1995) The unique radar scattering properties of silicic lava flows and domes. In: van Zyl J (ed) Sum Fifth Annual Airborne Earth Science Workshop Jet Propulsion Lab Publ 95-1:35–38

Ramsey MS, Fink JH, Christensen PR (1993) Thermal emission analysis of mineral glasses: application to remote sensing studies of Holocene silicic lava flows. Abstr of the IAVCEI Gen Assem, p 89

Ramsey MS, Fink JH (1994) Remote monitoring of volcanic domes: detection of chemical, textural and thermal heterogeneities. EOS Trans Am Geophys Union 75:716

Ramsey MS, Fink JH (1997) Remote determination of lava vesicularity: technique preparation for the upcoming spaceborne ASTER instrument. Abstract with Prog Geol Soc Am Cordilleran Sec 29:58

Ramsey MS, Christensen PR (1998) Mineral abundance determination: quantitative deconvolution of thermal emission spectra. J Geophys Res 103:577–596

Ramsey MS, Fink JH, Wessels R, Poland M, Ruff S (1998) Field spectroscopy and GPS analysis of silicic domes: implications for future volcanic monitoring with the spaceborne ASTER instrument. EOS Trans Am Geophys Union 79:1010

Realmuto VJ (1990) Separating the effects of temperature and emissivity: emissivity spectrum normalization. In: Abbott EA (ed) Proc Sec Ann Airborne Earth Sci Workshop Jet Propulsion Lab Publ 90 (55): 31–35

Realmuto VJ, Abrams MJ, Buongiorno MF, Pieri DC (1994) The use of multispectral thermal infrared image data to estimate the sulfur dioxide flux from volcanoes: a case study from Mount Etna, Sicily, July 29, 1986. J Geophys Res 99:481–488

Rosen PA, Hensley S, Zebker HA, Webb FH, Fielding EJ (1996) Surface deformation and coherence measurements of Kilauea Volcano, Hawaii, from SIR C radar interferometry. J Geophys Res 101:23109–23125

Rothery DA (1989) Volcano monitoring by satellite. Geol Today 11:1665–1667

Rowland SK, Smith GA, Mouginis-Mark PJ (1994) Preliminary ERS-1 observations of Alaskan and Aleutian volcanoes. Rem Sens Environ 48:358–369

Salisbury JW (1993) Mid-infrared spectroscopy: laboratory data. In: Pieters CM, Englert PA (eds) Remote geochemical analysis: elemental and mineralogical composition. Cambridge University Press, New York, pp 79–98

Sampson DE (1987) Textural heterogeneities and vent area structures in the 600-year-old lavas of the Inyo volcanic chain, eastern California. Geol Soc Am Spec Pap 212:89–101

Simon I, McMahon HO (1953) Study of some binary silicate glasses by means of reflection in infrared. J Am Ceram Soc 36:160–164

Thomson JL, Salisbury JW (1993) The mid-infrared reflectance of mineral mixtures (7–14 μm). Rem Sens Environ 45:1–13